NJC

Accepted Manuscript

ROYAL SOCIETY OF CHEMISTRY

www.rsc.org/njc

Journal Name

ARTICLE

One step synthesis of Ag-reduced graphene oxide-multiwalled carbon nanotubes for enhanced antibacterial activities

Leila Shahriary[a], Roopa Nair[b], Sushma Sabharwal[b], and Anjali A. Athawale[a*]

The present study reports one step rapid preparation of Ag nanoparticles decorated reduced graphene oxide-multiwalled carbon nanotube hybrids (Ag-rGO-MWCNTs) by heating the mixture of graphene oxide (GO), acid functionalized multiwalled carbon nanotubes (f-MWCNTs), and $AgNO_3$ aqueous solution in presence of NaOH at 80 °C without adding any external reducing agent. The product was characterized by Ultra violet-visible spectroscopy (UV-Vis), X-ray powder diffraction (XRD), and Energy-dispersive X-ray (EDX) analysis. Symmetrical shape of UV-Vis absorption peak at 398 nm indicates the presence of small and uniform sized Ag nanoparticles in case of Ag-rGO-MWCNTs. Moreover, the XRD peaks at 2θ ~38.1°, 44.2°, 64.5°, and 77.5° for the above mentioned composite suggest the formation of metallic Ag nanoparticles. Morphology of the sample was investigated using scanning electron microscope (SEM). The SEM images reveal that there is a lower degree of curls, folds, wrinkles and aggregation in case of Ag-rGO-MWCNTs. Further, the antimicrobial activity of Ag-rGO-MWCNTs was examined for *Escherichia coli* (*E. coli*) and *Bacillus subtilis*. Positive results were obtained only for *E. coli*. For comparison, silver nanoparticles decorated reduced graphene oxide (Ag-rGO) and multiwalled carbon nanotubes (Ag-MWCNTs) were prepared by similar method and after characterization, their antimicrobial activity towards Escherichia coli (*E. coli*) was also studied. Results indicate that Ag-rGO-MWCNTs has a superior antibacterial activity which may be due to the synergistic effect of rGO, MWCNTs and silver nanoparticles compared to that of Ag-rGO and Ag-MWCNTs. Also, the possible mechanism for antimicrobial activity of Ag-rGO-MWCNTs has been discussed.

Introduction

Silver nanoparticles (AgNPs) are well-known for bactericidal activity and biocompatibility amongst all the antibacterial nanomaterials [1-3]. It is well known that Ag nanoparticles and Ag nanocomposites are valuable biocides against several kinds of fungi, bacteria and viruses [2]. Hence, Ag nanoparticles find applications as antiseptic, disinfectant and pharmaceutical agents [4-6]. Studies have shown that the toxicity of Ag nanoparticles is size dependent and the smaller sized nanoparticles exhibit higher antibacterial activity, due to the high specific surface area and easy cell penetration [2, 3]. Therefore, mono-dispersed Ag nanoparticles with small size are desirable for the antibacterial control system. Nevertheless, the problem of particle aggregation and nanomaterial recovery are two big challenges while using Ag nanoparticles for various applications.

Graphene oxide (GO), a two-dimensional carbon material, has attracted a great deal of attention [7]. Apart from the layered structure with a large theoretical specific surface area [8] GO nano sheets contain abundant oxygen-containing surface groups, such as hydroxyl, epoxies, carbonyl and carboxyl groups [9]. The presence of such groups permit the GO sheets to be well dispersed in water to yield a stable suspension [10], and also provide nanoscale substrates for the fabrication of flexible GO based composite materials [11].

However, the formation of reduced GO in aqueous solution results in the aggregation of sheets due to hydrophobic nature and induces strong π–π interactions when the oxygen-containing functional groups are removed during the reduction process [12]. Important drawbacks in the synthesis of graphene are the difficulty in isolating single layer and its tendency to curl, fold and corrugate due to the flexibility of sheets [13]. As a result, graphene shows lower surface area and conductivity

compared to the predicted theoretical value. In addition, it has been found that GO and rGO exhibit strong antibacterial activity towards *Escherichia coli* (*E. coli*) [14-15]. The antibacterial activity of GO and rGO has been attributed to factors such as aggregation, size and membrane stress. Less aggregation and smaller size of GO nano sheets have higher toxicity than those with large size and higher degree of aggregation. Membrane stress induced by sharp edges of graphene nanosheets may result in physical damages on cell membranes, leading to loss of the bacterial membrane integrity and the leakage of RNA.

Hence, preparation of individual graphene sheets is rather critical. On the other hand, metal nanoparticles can interact with the GO sheets through electrostatic binding, physio sorption and charge-transfer interactions. Large GO sheets act as excellent supports and stabilizer [16] for the Ag nanoparticles, avoiding nanoparticles aggregation. Therefore, assembling the Ag nanoparticles on GO sheets can remarkably enhance the antibacterial activity.

Moreover, the antimicrobial activity of carbon nanotubes (CNTs) has been found to be the synergy of both "physical" and "chemical" effects [17]. Intensive physical interactions between CNTs and bacterial cells when they are in direct contact, may cause physical damages on cell membranes, and result in the release of intracellular contents [17-18]. At the same time, some "small" CNTs can enter the bacterial cells, while other "larger" CNTs aggregate, and may stick on the surface of bacterial cells [19-21]. It has been reported that the antimicrobial mechanism, proposed for carbon nanotubes, is applicable to graphene-based materials. As previously, proposed, cytotoxicity mechanism for the CNTs and graphene based material are parallel [17, 22].

However, aggregation of nanomaterials such as CNTs, graphene, rGO, and fullerenes significantly influence the interactions between nanoparticles and bacteria. Therefore, smart and distinctive hybrid materials containing AgNPs, graphene, and CNTs could overcome limitations of individual components such as aggregation, uniform distribution of nanomaterials, and may also be cost effective.

The present paper shows one-pot approach towards the rapid synthesis of silver deposited on reduced graphene oxide-multiwalled carbon nanotubes (Ag-rGO-MWCNTs). The formation of Ag-rGO-MWCNTs is accomplished by directly heating the mixture of GO, acid functionalized MWCNTs (f-MWCNTs) and $AgNO_3$ aqueous solution in the presence of sodium hydroxide at 80 °C for 10 min under stirring condition without using additional reducing agent and a surface modifier. It seems that GO and f-MWCNTs act as reducing agents for the formation of AgNPs while, GO and f-MWCNTS can be converted into rGO and MWCNTs respectively at the same time under alkaline conditions. Further, Ag-MWCNTs and Ag-rGO nanocomposites have been synthesized by similar method and antimicrobial activity of all three composites have been studied using *E. coli* and *Bacillus subtilis* as a source of bacteria. Positive results are obtained for *E. coli*. Results indicate that Ag-rGO-MWCNTs have higher antimicrobial

activity towards *E. coli* compared to other two silver nanocomposites at all the studied concentrations.

Experimental

Reagents

Graphite powder, $NaNO_3$ (99%), NaOH, H_2O_2 (30%), $KMnO_4$ (99%) and $AgNO_3$ (99%) were purchased from Sigma-Aldrich (USA). MWCNTs were obtained from Reinste Nano Ventures Pvt. Ltd, New Delhi, India. Concentrated H_2SO_4 (96%), concentrated HCl (36%), NaCl (99%) and HNO_3 (70%) were obtained from SD-Fine Chemical (SDFCL) (India). All the chemicals were of analytical reagent grades and used as received, without further purifications. *Escherichia coli* (NCIM no 2563) and *Bacillus subtilis* (NCIM no 2063) were supplied by National Chemical Laboratory (NCL) Pune; Luria Bertani (LB) and McFarland standards were purchased from Hi media (India). HeLa (Human epithelial carcinoma cell line) cell line was obtained from National Center for Cell Science, Savitribai Phule Pune University, Pune, India.

Synthesis of GO

Graphene oxide (GO) was synthesized from graphite powder using modified Hummer's method [23]. In brief, 1 g of graphite and 0.5 g of sodium nitrate were added in 23 mL of concentrated sulphuric acid under constant stirring. $KMnO_4$ (2 g) was added gradually to the above solution while keeping the temperature less than 20 °C to prevent overheating and explosion. The mixture was stirred at 35 °C for 1 h and the resulting solution was diluted by adding 100 mL of water under vigorous stirring. To ensure the completion of reaction with $KMnO_4$, after 12 h constant stirring the suspension was further treated with 30% H_2O_2 solution (5 mL). The resulting mixture was washed with HCl and H_2O respectively, followed by filtration and drying the graphene oxide sheets thus obtained.

Synthesis of acid functionalized multiwalled carbon nanotubes

Acid (-COOH) functionalized MWCNTs (f-MWCNTs) were prepared by refluxing purified MWCNTs in concentrated HNO_3 (ca. 15.8 M) for 8 h.

Synthesis of Ag-rGO-MWCNTs, Ag-MWCNTs, and Ag-rGO

Composite of Ag-rGO-MWCNTs, was synthesized by initially taking 20 mL of aqueous dispersion of carbon nanomaterials (GO and f-MWCNTs 0.5 mg mL^{-1}) containing 3 mM $AgNO_3$ in a beaker. The solution was heated to 80 °C under constant stirring followed by drop wise addition of 2.0 mL of 8 M NaOH aqueous solution. After complete addition of NaOH the reaction mixture was stirred for 10 min and then washed with water after centrifugation till the filtrate showed neutral pH. The product was dried in oven at 80 °C for 12 h [24]. Ag-MWCNTs and Ag-rGO were prepared by similar method using dispersion of 1 mg mL^{-1} MWCNTs and rGO respectively. The

composites were characterized by using UV-Vis, SEM and XRD analysis**.**

Characterization of samples

Ultra violet visible (UV-Vis) spectra of samples were recorded on Perkin Elmer LAMBDA 950 spectrophotometer. Powder X-ray diffraction (XRD) analyses of the samples were carried out on a Bruker D8 (with Cu Kα) X-ray diffractometer. Micro Raman spectra of the samples were recorded by using Horiba Jobin Yvon (France Instrument), at 532 nm laser power 1.7 mW, 100x objective lens and 0.9 NA. Scanning electron microscope (SEM) images were recorded on JEOL JSM-6360 microscope. Optical density was measured by digital calorimeter EQ-650A.

Antimicrobial activity test:

Bacterial Culture

E. coli was chosen as the model pathogen for antibacterial activity experiments. *E. coli* were cultivated in Luria-Bertani nutrient broth at 37 ℃ for 24 h to get the exponential growth phase. The cells were collected by centrifugation and washed with saline solution (0.85% NaCl, pH 7) and then re-suspended in physiological saline (0.85%, NaCl) solution to maintain the concentration of 10^7-10^8 colony forming units (CFU mL^{-1}). The optimal density of bacterial cells was adjusted to 0.5 McFarland standards. All the glass apparatus and solutions used in the experiments were autoclaved at 121 ℃ for 20 min to maintain sterile conditions.

Measurement of minimum inhibitory concentration (MIC)

The above mentioned bacterial culture was used for initially determining the minimum inhibitory concentration of the nanomaterial. The minimum inhibitory concentration (MIC) is defined as the lowest concentration of material that inhibits the growth of an organism. Different concentrations of Ag-rGO, Ag- MWCNTs, and Ag-rGO-MWCNT, dispersion (0, 5, 10, 15, 20 and 25 μg mL^{-1}) were added in LB broth. The density of *E. coli* cell was adjusted to 10^7- 10^8 CFU mL^{-1} and then inoculated into the above nanocomposites suspension followed by incubation at 37 ℃. Bacterial growth was measured as the increase in absorbance at 600 nm. The experiments also included a positive control (flask containing nanocomposites and nutrient media, devoid of inoculums) and a negative control (flask containing inoculums and nutrient media, devoid of nanocomposites).

Cell Viability test of *E. coli* with Ag-rGO, Ag-MWCNTs, and Ag-rGO-MWCNTs

The antimicrobial activities of samples were investigated with the help of cell viability test of *E. coli* by using the above mentioned bacterial culture. For this, experiments were carried out by using two different concentrations of samples (viz. 25 and 15 μg mL^{-1}) of Ag-rGO, Ag-MWCNTs, and Ag-rGO-MWCNTs respectively.

E. coli (10 μL) cells were transferred to 1 mL of the test solution (25 and 15 μg mL^{-1} Ag-rGO, Ag-MWCNTs, or Ag-rGO-MWCNTs) in a test tube. These tubes were incubated at 37 ℃ with intermittent mixing after every 15 min for 2 h. The viability of E. coli cells was evaluated by the colony count method. Briefly, the above mixtures were diluted with a gradient method and spread on to LB plates, and left to grow overnight (24 h) at 37 ℃. Colonies were counted, and compared to those on control plates to calculate the cell growth inhibition. All treatments were prepared in duplicate and repeated at least thrice to check the reproducibility. Corresponding controls without any dispersion were run simultaneously.

Loss of viability was calculated by the following equation (1):

$$\text{Loss of viability \%} = [Cc - Cs/ Cc] \times 100 \qquad (Eq.1)$$

where Cc is colony count of control, and Cs is colony count of samples after incubation with suspensions.

The effect of time on cell viability was studied by adding 10 μl of *E. coli* cells into nanocomposite viz Ag-rGO, Ag-MWCNTs, or Ag-rGO-MWCNTs dispersion of concentration 20 μg mL^{-1}, 20 μl of above mixture was spread after every hour on Luria-Bertani agar plates and the loss of viability of *E. coli* was counted upto 4 h.

The morphological changes of E. coli on treatment with Ag-rGO, Ag-MWCNTs, Ag-rGO-MWCNTs were observed with a scanning electron microscope (SEM). Bacterial cells were harvested after the exposure, fixed in glutaraldehyde (2.5% v/v phosphate buffer, pH 7.2) and dehydrated by sequential treatment with 50, 60, 70, 80, 90, 95, and 100% ethanol for 15 min. The dried cells were sputter-coated with platinum for SEM imaging.

Cell culture

Hela cell line was cultured in Dulbecco's Modified Eagle Medium (DMEM). Cultured media were supplemented with 10% fetal calf serum and 1% antibiotic solution. The cells were grown in humidified atmosphere containing 5% CO$_2$ at 37 °C for 24 h.

Cytotoxicity activity

Cell viability was evaluated by the 3-(4, 5-dimethylthiazol- 2-yl)-2,5-diphenyltetrazolium bromide (MTT colorimetric technique). This assay is based on the metabolic reduction of soluble MTT by mitochondrial enzyme activity of viable cells into an insoluble colored formazan product, which can be measured spectrophotometrically after dissolving in DMSO. Hela cancer cell lines were seeded in well tissue culture plates. Stock solution of nanocomposites (Ag-rGO, Ag-MWCNTs, and Ag-rGO-MWCNTs) were prepared in sterile distilled water and diluted to required concentration (25-250 μg mL^{-1}) using cell

culture medium. Appropriate concentration of nanocomposites stock solution were added to the cultures to obtain respective concentration of nanocomposites and further incubated for 24, 48, 72 and 96 h, and MTT assay was carried out. The MTT solution (20 μL, 5 mg mL^{-1}) prepared in 10 mM phosphate buffer was added to each well and incubated for 4 h. The purple formazan product was dissolved by addition of 100 μL of 100% DMSO for 5 min. The plates were placed on shaker for 15 min to complete solubilisation of crystal, and the optical density of each well was determined. The amount of formazan product was measured by measuring absorbance, as it is directly proportional to the number of living cells in culture. The absorbance was measured at 570 and 630 nm using an ELISA plate reader, and the viability was calculated. Data were collected for three replicates each and were used to calculate the mean. The percentage inhibition was calculated from this data by equation 2:

% Inhibition = Mean OD of untreated cells (control)/ Mean OD of treated cells (control) × 100   (Eq.2)

Cytomorphological changes in Hela cells by nanocomposites

Hela cells (1× 10^5 cells/well) were seeded in a 6 well plate for 24 h. After 24 h, they were treated with nanocomposites (concentration 50 μg/ml) and incubated for 48 h at 37 °C in 5% CO_2 atmosphere. The treated cover slips were transferred into another 6-well plate where the cells were fixed with 1% paraformaldehyde. Cover slips were washed with PBS, dipped in alcohol and allowed to dry. Further, the coverslip was dipped in xylene and mounted using distrene plasticizer xylene (DPX). The images were taken in a Carl Zeiss Axio Scope A1 fluorescent microscope in the bright field mode.

Results and discussion

Material characterization

Ag-rGO-MWCNTs, Ag-rGO, Ag-MWCNTs, composites were prepared by heating the mixture of GO, MWCNTs (0.5 mgmL^{-1}) and AgNO$_3$ (3 mM) aqueous solution in the presence of sodium hydroxide (2.0 mL of 8 M) at 80 °C under constant stirring. The reaction was completed in 10 min without extra reducing agent [25]. Fig.1.A shows the UV-Vis spectra of GO, MWCNTs, GO+MWCNTs (physically mixture), Ag-rGO, Ag-MWCNTs, and Ag-rGO-MWCNTs composites.

The peak observed at 230, 260 and 235 nm (spectrum a, b and c dashed line) for GO, f-MWCNTs and GO+f-MWCNTs respectively represents the π-π* transitions of C-C aromatic ring, while the shoulder at ~308 nm in case of GO and GO+f-MWCNTs (a, and c dashed line) corresponds to n-π* transition of C=O bond [25-26]. In contrast, the UV-Vis spectrum of the Ag-rGO, Ag-MWCNTs and Ag-rGO-MWCNTs composites (a, b, c solid line respectively) display an absorption band at about 420, 406, and 398 nm, respectively which is the characteristic absorption band of Ag nanoparticles due to Plasmon resonance [27], indicating that Ag nanoparticles are deposited on the GO, MWCNTs and rGO-MWCNTs nanomaterials. According to the Mie theory, when the solution system is mono-dispersed

(narrow size distribution) the peak shape is symmetric and the value of the full width at half maximum (FWHM) is small.
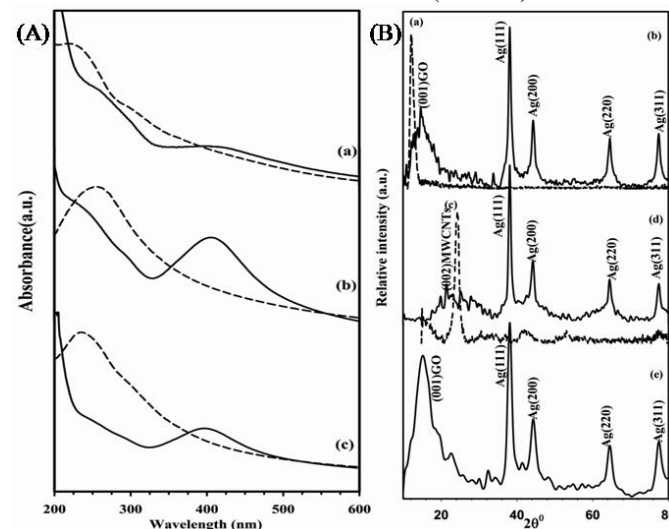

Fig.1. (A) UV-Vis spectra of, dashed line (a) GO, (b) MWCNTs, (c) GO+MWCNTs and solid line (a) Ag-rGO, (b) Ag-MWCNTs, and (c) Ag-rGO-MWCNTs. (B) XRD patterns of (a) GO, (b) Ag-rGO, (c) MWCNTs, (d) Ag-MWCNTs, and (e) Ag-rGO- MWCNTs

When the system is poly-dispersed, the peak shape is asymmetric, which suggests that the peak actually consists of two or more absorption peaks of different species [28]. The UV-Vis absorption peak at lower wavelength with symmetrical shape in case of Ag-rGO-MWCNTs indicates the smaller and uniform size of the anchored Ag nanoparticles compared to Ag-rGO, and Ag-MWCNTs.

The X-ray diffraction (XRD) patterns of GO (a), Ag-rGO (b), f-MWCNTs (c), Ag-MWCNTs (d), and Ag-rGO-MWCNTs (e) composites are represented in Fig. 1B. The diffraction peak at 2θ ~ 12.1° (Fig.1B, a) can be attributed to the 001 plane of GO and that at ~ 24.05° (Fig.1B, c) correspond to 002 plane of MWCNTs, the presence of similar peaks (with positive shift) in the Ag-rGO (~14.05°), and Ag-MWCNTs (broad peak ~23°-25°) confirm the presence of respective species in the composites. Furthermore, two peaks at 2θ~14.8° and ~26.08° (Fig.1B, e) verify the presence of rGO and MWCNTs in Ag-rGO-MWCNTs composite. Moreover, the peaks at 2θ ~38.1°, 44.2°, 64.5°, and 77.5° for above mentioned composites (Fig.1B. a, b, c) can be respectively indexed to the 111, 200, 220, and 311 diffractions of face centred cubic (fcc) structure of metallic silver (JCPDS No. 04-0783), suggesting the formation of metallic Ag nanoparticles. The average size of Ag nanoparticles has been calculated using Scherrer equation (2) for each sample by considering Ag 111 plane.

$$D = \frac{K\lambda}{\beta\cos\theta}$$

(Eq.2)

where D is the crystallite size, λ is wavelength of the Cu Kα used, β is the full width at half maximum of the diffraction peak, K is the shape factor (0.94) and θ is the angle of

diffraction. The crystallite size of ~ 118, 95, and 52 nm are obtained for Ag nanoparticles for Ag-rGO, Ag-MWCNTs and Ag-rGO-MWCNTs composites respectively. The values obtained are comparable with those obtained from SEM images.

Fig.2A illustrates the typical micro Raman spectra of f-MWCNTs, GO, Ag-rGO, Ag-MWCNTs, and Ag-rGO-MWCNTs samples obtained at an excitation wavelength of 532 nm. Three distinct peaks are observed in each sample at ~1340, ~1540 and ~ 2650 cm-1 corresponding to D band, G band and 2D band, respectively. In the Raman D/G and 2D/D+G intensity ratios (I_D/I_G and I_{2D}/I_{D+G}) are usually used to evaluate the average size of crystalline sp^2 domains and defect densities in graphene sheets. However, the I_D/I_G and I_{2D}/I_{D+G} ratios of Ag-rGO-MWCNTs hybrid (1.67 and 3.30, respectively) are remarkably greater than those of GO (1.13 and 1.42), and f-MWCNTs (1.00 and 1.41), Ag-MWCNTs(1.32, 2.85), and Ag-rGO(1.41, 3.04) indicating higher degree of topological disorder and defect density together with higher degree of crystallinity within Ag-rGO-MWCNTs hybrid material in which more number of smaller sized graphitic demined are present. The broader width of D and G bands in case of Ag-rGO-MWCNTs, Ag-rGO, and Ag -MWCNTs, compared to that of GO, and f-MWCNTs may be due to deposition of Ag nanoparticles [29].

In addition, absence of characteristic peaks for Ag+ in XRD and Raman spectra (at 32.5° attributed to 111 plane of Ag_2O (JCPDS 761393) in XRD and at 1068 cm^{-1} in Raman spectra [30] confirm the absence of Ag+ and presence of Ag nanoparticles.

Fig.3. SEM micrographs of (a) Ag-rGO, (b) Ag-MWCNTs, and (c) Ag-rGO-MWCNTs. Particle size distribution (a1) for Ag-rGO, (b1) Ag-MWCNTs, (c1) Ag-rGO-MWCNTs.

The SEM images of Ag-rGO, Ag-MWCNTs, and Ag-rGO-MWCNTs are represented in Fig. 3 a, b, and c respectively. Comparison of micrographs [Fig. 3a, (Ag-rGO) and Fig. 3b (Ag-MWCNTs) with the Fig. 3c (Ag-rGO-MWCNTs)], reveal that there is lower degree of curls, folds, wrinkles and aggregation in case of Ag-rGO-MWCNTs which is possibly due to insertion of MWCNTs between the GO layers during the reduction reaction, also, it is important to note that by changing the type of carbon nanomaterial as a support, the size of Ag nanoparticles also change and smaller sized Ag nanoparticles are formed in case of Ag-rGO-MWCNTs composite (Fig. 3 a1, b1, and c1).

The plots of energy-dispersive X-ray (EDX) analysis together with the table for the elemental composition for Ag-rGO, Ag-MWCNTs, and Ag-rGO-MWCNTs composites are shown in Fig. s1, s2, s3 and s4 respectively. The percentage of silver is found to be lower in Ag-rGO-MWCNTs composite compared to that of Ag-rGO and Ag-MWCNTs as observed from Fig. s4.

Antibacterial activity of Ag-rGO, Ag-MWCNTs and Ag-rGO-MWCNTs

E. coli and *Bacillus subtilis* were used as the model bacteria to evaluate the antibacterial activities of different nanocomposites (Ag-rGO, Ag-MWCNTs and Ag-rGO-MWCNTs). However, it was observed that Ag-rGO, Ag- MWCNTs and Ag-rGO-MWCNTS exhibited appreciable antibacterial effect against *Bacillus subtilis,* at relatively very high concentrations (500 µg mL^{-1}) but they showed good antibacterial activity against *E. coli* even at very low concentrations. Hence the cell viability and antibacterial potential of the nanocomposites was studied against *E. coli* at different concentrations.

The antibacterial activity of the nanocomposites is found to be dependent on their concentrations and the initial bacterial concentration [31]. To study the effect of concentration on the anti-bacterial activity, dispersions of Ag-rGO, Ag-MWCNTs and Ag-rGO-MWCNTs with varying concentrations (5, 10, 15, 20, and 25 µg mL^{-1}) were incubated with a fixed concentration of *E. coli* cells (10^7-10^8 $CFUmL^{-1}$), the absorbance of each suspension was measured at 600 nm.
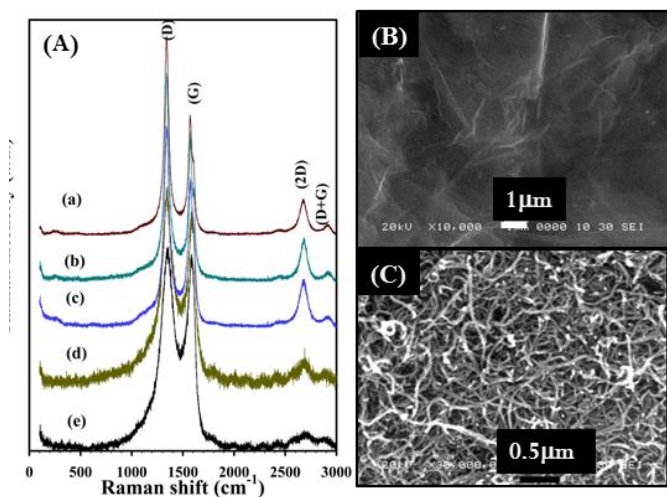

Fig.2.(A) Raman spectra of (a)f-MWCNTs (b)GO (c) Ag-MWCNTs (d) Ag-rGO and (e) Ag-rGO-MWCNTs. SEM images of (B) GO and (C) MWCNTs.

SEM was used to analyze the morphology of the sample. Fig. 2a shows the SEM image of GO with curl, folds and corrugation which is due to the flexibility of sheet and Fig. 2b, depicts the SEM images of MWCNTs with entangled and aggregated tubular structure.
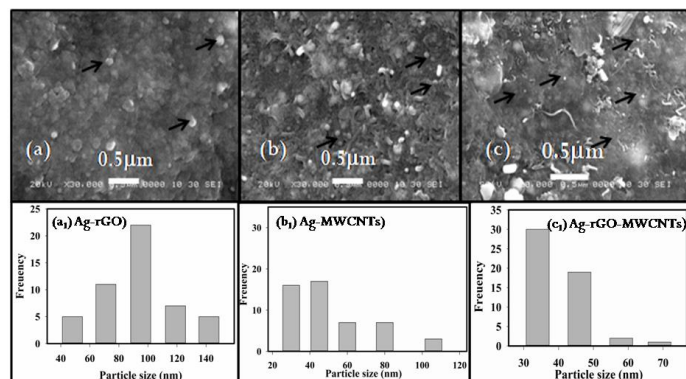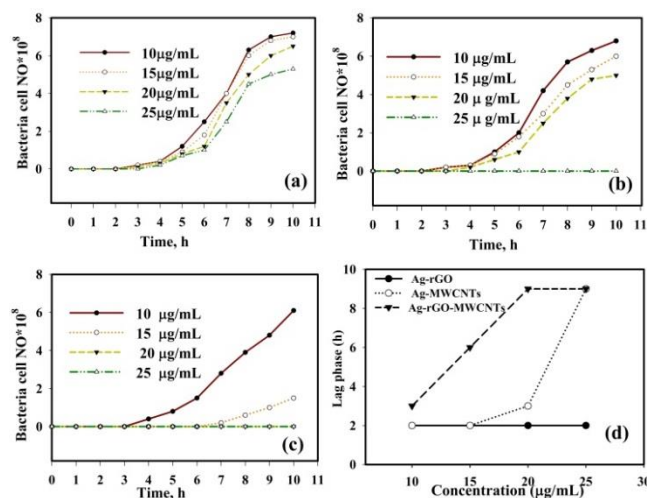
New Journal of Chemistry Accepted Manuscript

Fig.4. Batch growth profile in presence of various concentrations of (a) Ag-rGO, (b) Ag-MWCNTs and (c) Ag-rGO-MWCNTs. (d) lag phase vs. different concentrations of nanocomposites.

Fig.4 depicts the batch growth profiles for each of the composites. As observed from the Figure, the lag phase is seen to increase while absorbance at λ_{max} (represent the number of bacteria) decreases as a function of concentration of nanocomposites. Similar observations have been reported by Sondi et al. [32] in their studies on effect of silver nanoparticles on a single strain of E. coli. As the concentration of nanoparticles increased to MIC of the respective strains, the growth of bacteria was observed to be terminated. In the present study, Ag-rGO shows a lag phase of ~2 h irrespective of the nanoparticles concentration, while, the MIC is found to be 20 µg mL^{-1} for Ag-MWCNTs, with a 3 h lag phase and 15 µg mL^{-1} for Ag-rGO-MWCNTs with a 6 h lag phase respectively (Fig. 4d). Therefore, the results indicate that Ag-rGO-MWCNTs shows highest antimicrobial activity towards *E-coli* compared to other nanocomposites.
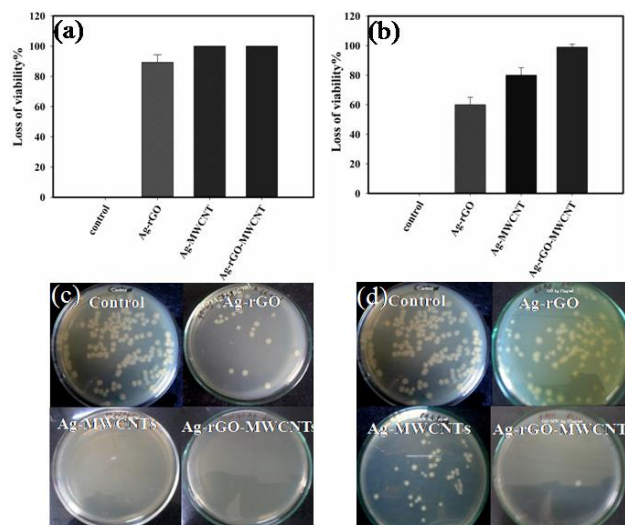

Fig.5. Cell viability of bacterial cells by colony count method for the bacteria treated with Ag-rGO, Ag-MWCNTs and Ag-rGO-MWCNTs at concentration of (a, c) 25 and (b, d) 15 µg mL^{-1}.

Cell viability of bacterial cells was determined by colony count method as described in material and methods and the isotonic solution without any dispersion was used as control. 25 µg mL^{-1} of Ag-rGO, Ag-MWCNTs and Ag-rGO-MWCNTs dispersion in an isotonic solution were incubated with *E. coli* cells (10^7 - 10^8 CFU mL^{-1}) at 37 °C for 2 h. The results demonstrated that after treating the bacteria with Ag-rGO, Ag-MWCNTs and Ag-rGO-MWCNTs dispersions the loss of viability was found to be very high, 89±5% for Ag-rGO, and 100% for the remaining two composites (Fig. 5a, and c). Therefore, experiments were carried out by treating the bacteria with lower concentration i.e. 15 µg mL^{-1} of the composites. The results showed that the loss of viability is almost retained to 100% (99+2.1%) for Ag-rGO-MWCNTs and decreased significantly to 60 ± 5.2%, and 80 ± 4.3% for Ag-rGO and Ag-MWCNTs respectively (Fig. 5b and d).Based on these observations, the time dependent antibacterial behaviour was investigated for Ag-MWCNTs, and Ag-rGO-MWCNTs composites. For this, 20 µg mL^{-1} of Ag-MWCNTs and Ag-rGO-MWCNTs dispersions were incubated with E. coli upto 4 h and the viability was counted at an interval of 1 h.

As observed from Fig.6, 100% loss of viability is achieved for Ag-rGO-MWCNTs after 2 h while for Ag-MWCNTs it is found to be after 3 h. These results indicate that the Ag-rGO-MWCNTs composite exhibits highest antibacterial activity in comparison to the other composites (Ag-rGO, Ag-MWCNTs).
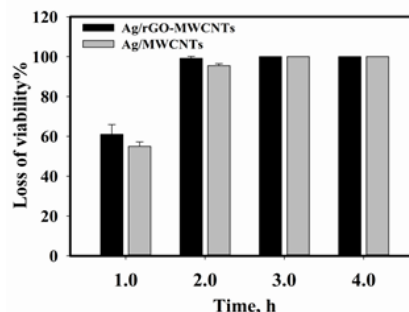

Fig.6. Time dependent antibacterial activities of Ag-MWCNTs and Ag-rGO-MWCNTs upto four hours incubation.

The effects of the composites on the bacterial cell were investigated by recording the scanning electron micrographs of the bacteria before and after the treatment with the nano composites.
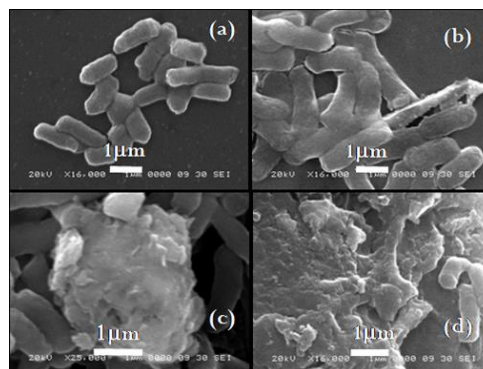

Fig.7. E. coli bacterium cell (a) before and after treatment with 15 µg mL^{-1} of (b) Ag-rGO, (c) Ag-MWCNTs, and (d) Ag-rGO-MWCNTs for two hours.

Fig.7 shows the micrographs of E. coli before (Fig.7a) and after treatment with 15 µg mL-1 of Ag-rGO (Fig.7b), Ag-MWCNTs (Fig. 7c), and Ag-rGO-MWCNTs (Fig. 7d) for 2 h. The E. coli bacterium cell shows a rod shape structure with intact surface as observed from the Fig. 7a. On the other hand, in case of treated samples (Fig.7 b, c, and d) the cells are seen to be damaged in the sequence as Ag-rGO < Ag-MWCNTs < Ag-rGO-MWCNTs respectively. These results confirm the superior antibacterial activity of Ag-rGO-MWCNTs composite which can be attributed to the synergistic effect of each constituent present in the composite i.e. rGO, MWCNTs, and Ag nanoparticles.

Further, it has been reported that shorter length of carbon nano tubes increases the probability of interaction between the bacterial cells and the nanotubes since the interaction occurs between the cell and the open end of nanotubes [33]. Similarly, the graphene based materials interact with the bacterial cells through the edges of layers. The Ag-MWCNTs and Ag-rGO composites also interact with the bacterial cell by similar mechanism with the antibacterial activity being enhanced due to the presence of silver nanoparticles [34-35]. The antibacterial activity involves three steps: In the first step the bacterial cells gather and adsorb on the surface of composites which may enhance the interaction between the bacteria and Ag nanoparticles. In the second step the Ag nanoparticles, tips of the tubes and edges of layers damage the bacterial cell wall followed by the complete disintegration of the cell [17, 22].

In case of Ag-rGO-MWCNTs composite antimicrobial activity is highest compared to that of Ag-rGO and Ag-MWCNTs composites due to the following reasons: i) presence of both, MWCNTs and rGO sheets which cause less aggregation, as shown in Fig. 3c. ii) availability of higher number of edges of rGO and tips of MWCNTs for direct contact with bacterial cells and iii) presence of smaller sized Ag nanoparticles on the rGO-MWCNTs hybrids.
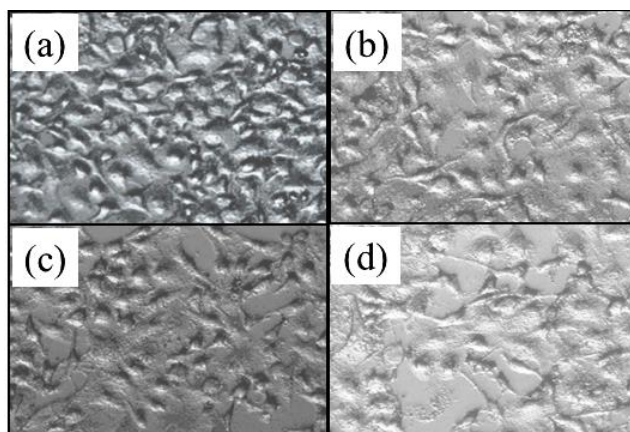
Cytotoxic activity

Fig.8. Hela cells (a) before treatment (control) and after treatment with (b) Ag-rGO, (c) Ag-MWCNTs, and (d) Ag-rGO-MWCNTs for one hour.

MTT assay was used to assess the effect of Ag-rGO, Ag-MWCNTs and Ag-rGO- MWCNTs on the cytotoxicity of Hela cell lines. The cells were incubated with different concentrations of nanoparticles (Ag-MWCNTs, Ag-rGO, Ag-rGO- MWCNTs) viz. 25, 50, 100, 200, and 250µg. All three above mentioned nanocomposites inhibit the viability of Hela

cancer cell lines in dose and time dependent manner (S5).The nanocomposites showed more than 90% viability at 24 h of incubation, as the incubation time was increased the cell viability decreased. This result suggests that these nanoparticles are not cytotoxic at lower concentration and at lower incubation time.

Cytomorphological changes of Hela cells induced by the nanocomposites

The Hela cells (a) were treated with Ag-rGO (b), Ag-MWCNTs (c) and Ag-rGO- MWCNTs (d) at 50 µg/ml concentration for 24 h. Fig 8d shows that there are no significant morphological changes in case of Hela cells treated with Ag-rGO-MWCNTs.

Conclusions

Composites of silver nanoparticles decorated reduced graphene oxide, silver nanoparticles decorated multiwalled carbon nanotube and silver nanoparticles decorated reduced graphene oxide-multiwalled carbon nanotube hybrids have been obtained by one step rapid preparation method. The results of the different composites reveal that the silver decorated multiwalled carbon nanotube hybrid are showing highest antibacterial activity towards E.coli compared to other composites. The antibacterial activity was found to be time as well as concentration dependent. Further, the cytotoxicity studies suggest that the nanocomposites are not cytotoxic to Hela cells at lower concentrations and at lower incubation time. These results can be due to synergistic effect of reduced graphene oxide, multiwalled carbon nanotubes and Ag nanoparticles.

Acknowledgements

Notes and references

a Department of Chemistry, University of Pune, Ganeshkhind, Pune 411007, India.

b Division of Biochemistry, Department of Chemistry, University of Pune, Ganeshkhind, Pune 411007, India.

1   M. L. W. Knetsch, L. H. Koole, *Polymers*, 2011, **3**, 340.

2   C. Marambio-Jones, E. M. V. Hoek, *J. Nanopart. Res.,* 2010, **12**, 1531.

3   J. R. Morones, J. L. Elechiguerra, A. Camacho, K. Holt, J. B. Kouri, J. T. Ramirez, M. J. Yacaman*, Nanotechnology,* 2005, **16**, 2346.

4   A. Kumar, P. K. Vemula, P. M. Ajayan, G. John, *Nat. Mater.,* 2008, **7**, 236.

5   V. A. Oyanedel-Craver, J. A. Smith, *Environ. Sci. Technol.,* 2008, **42**, 927.

6   S. Pal, E. J. Yoon, Y. K. Tak, E. C. Choi, J. M. Song, *J. Am. Chem. Soc.,* 2009, **131**, 16147.

7   A. K. Geim, K. S. Novoselov, *Nature Mater,* 2007, **6**, 183.

8   L. L. Zhang, R. Zhou, X. S. Zhao, *J. Mater. Chem.,* 2010, **20**, 5983.

9   I. V. Lightcap, T. H. Kosel, P. V. Kamat, *Nano Lett.,* 2010, **10**, 577.

10   S. Stankovich, D. A. Dikin, G. H. B. Dommett, K. M. Kohlhaas,E. J. Zimney, E. A. Stach, R. D. Piner, S. T. Nguyen, R. S. Ruoff, *Nature,* 2006, **442**, 282.

11   S. Niyogi, E. Bekyarova, M. E. Itkis, J. L. McWilliams, M. A. Hamonand R C. Haddon, *J. Am. Chem. Soc.,* 2006, **128**, 7720.

12   P. V. Kamat, *J. Phys. Chem. Lett.,* 2010, **1**, 520.

13   W. Yang, K. R. Ratiniac, S. P. Ringer, P. Thordarson, J. J. Gooding, F. Braet, *Angew. Chem.,* 2010, **49**, 49.

14   W. Hu, C. Peng, W. Luo, M. Lv, X. Li, D. Li, Q. Huang, C. Fan, *ACS Nano,* 2010, **4**, 4317.

15   O. Akhavan, E. Ghaderi, *ACS Nano,* 2010, **4**, 5731.

16   R. Muszynski, B. Seger, P. V. Kamat, *J. Phys. Chem. C.,* 2008, **112**, 5263.

17   C. D. Vecitis, K. R. Zodrow, S. Kang, M. Elimelech, *ACS Nano,* 2010, **4**, 5471.

18   S. Kang, M. Herzberg, D. F. Rodrigues, M. Elimelech, *Langmuir,* 2008, **24**, 6409.

19   S. B. Liu, A. K. Ng, R. Xu, J. Wei, C. M. Tan, Y. H. Yang, Y. Chen, *Nanoscale,* 2010, **2**, 2744.

20   S. Kang, M. Pinault, L. D. Pfefferle, M. Elimelech, *Langmuir,* 2007, **23**, 8670.

21   H. Wang, L. Gu, Y. Lin, F. Lu, M. J. Meziani, P. G. Luo, W. Wang, L. Cao, Y. P. Sun, *J. Am. Chem. Soc.,* 2006, **128**, 13364.

22   S. Liu, T. H. Zeng, M. Hofmann, E. Burcombe, J. Wei, R. Jiang, J. Kong, Y. Chen, *ACS Nano,* 2011, **5**, 6971.

23   K. Krishnamoorthy, R. Mohan, S.J. Kim, *Appl. Phys. Lett.,* 2011, **98**, 244101.

24   J. Tian, S. Liu, Y. Zhang, H. Li, L. Wang, Y. Luo, A. M. Asiri, A. O. Al-Youbi, X. Sun. *Inorg. Chem.,* 2012, **51**, 4742.

25   K. Krishnamoorthy, V. Murugan, R. Mohan, S. J. Kim, *Appl. Phys. A.,* 2012, **106**, 501.

26   Z. Xu, N. Gao, S. Dong, *Talanta,* 2006, **68**, 753.

27   J. Ma, J. Zhang, Z. Xiong, Y. Yong, X. S. Zhao, *J. Mater. Chem.,* 2011, **21**, 3350.

28   Y. J. Xiong, Y.N. Xia, *Adv. Mater.,* 2007, **19**, 3385.

29   W. Yuan, G. Jiang, J. Che, X. Qi, R. Xu, M. W. Chang, Y. Chen, S. Y. Lim, J. Dai,| M. B. Chan-Park, *J. Phys. Chem. C* 2008, **112**, 18754

30   G. R. I. N. Waterhouse, G. A. Bowmaker, J. B. Metson, *Phys. Chem. Chem. Phys.*, 2001, **3**, 3838.

31   S. Pal, Y. K. Tak, J. M. Song, *Appl. Environ. Microbiol.,* 2007, **73**, 1712.

32   I, Sondi, B. Salopek-Sondi, *J Colloid Interf Sci.,* 2004, **275**, 177.

33   J. Zhang, S. Srivastava, R. Duffadar, J. M. V. Davis, M. Rotello, M. M. Santore, *Langmuir,* 2008, **24**, 6409.

34   V. K. Rangari, G. M. Mohammad, S. Jeelani, A. Hundley, K. Vig, S. R. Singh, S. k. Pillai, *Nanotechnology,* 2010, **21**, 095102.

35   L. Liu, J. Liu, Y. Wang, X. Yan, D. D. Sun, *New J. Chem.,* 2011, **35**, 1418.

New Journal of Chemistry Accepted Manuscript